Title	First-principles study of the excited-state properties of coumarin-derived dyes in dye-sensitized solar cells
Authors(s)	Agrawal, Saurabh, Dev, Pratibha, English, Niall J., Thampi, Ravindranathan, MacElroy, J. M. Don
Publication date	2011-06-23
Publication information	Agrawal, Saurabh, Pratibha Dev, Niall J. English, Ravindranathan Thampi, and J. M. Don MacElroy. "First-Principles Study of the Excited-State Properties of Coumarin-Derived Dyes in Dye-Sensitized Solar Cells" 21, no. 30 (June 23, 2011).
Publisher	RSC publishing
Item record/more information	http://hdl.handle.net/10197/3016
Publisher's version (DOI)	10.1039/C1JM10953G

First-principles study of excited-state properties of coumarin-derived dyes in dye-sensitized solar cells

Saurabh Agrawal, Pratibha Dev, Niall J. English,[*] **K. Ravindranathan Thampi**[*] **and J. M. D. MacElroy**

Using Time-Dependent Density Functional Theory (TD-DFT), we have investigated the optical properties of dye-sensitized solar cells (DSSCs) comprised of TiO_2 nanoparticle sensitized with two coumarins, namely, NKX-2311 and NKX-2593. The two sensitizers (dyes) differ only in their linker moieties and are shown to have different absorption spectra when adsorbed on to the TiO_2 surface. Knowledge of different light absorption and charge transfer (CT) behavior within these complexes is useful for further improving the photo-dynamics of newer organic dyes presently being designed and investigated worldwide. Moreover, we have also investigated the effect of deprotonation of the sensitizers' carboxylic groups during adsorption on the titania surface and the excited state electronic properties of the resulting species.

1   Introduction

Solar cells rely on resources that are not only sustainable, but are relatively much cleaner compared to the burning of fossil fuels. Although efficient, silicon based solar cells are very expensive due to the high level of purity required to make solar-grade silicon. The search for low-cost, efficient solar cells has inspired a great deal of interest in dye-sensitized solar cells (DSSCs) based on much cheaper metal oxides such as TiO_2.[1] A typical DSSC is composed of a mesoporous semiconductor metal oxide, an adsorbed layer of sensitizers (dye) on the semiconductor surface, an electrolyte, and a counter electrode. The surface adsorbed sensitizers are excited by incident light energy. Electron injection into the conduction band of the semiconductor takes place by photo-oxidation of the sensitizer molecule. The sensitizer returns to its neutral ground state through an I/I_3^- redox couple present in the system as electrolyte.[2] The overall cell efficiency depends on several factors. For example, the electron from the conduction band can recombine with the photo-oxidized dye molecule or redox mediator in the electrolyte solution, thereby reducing the cell performance.[3] Also, the efficiency of the electron transfer from sensitizer to the semiconductor conduction band depends upon the excited state redox potential, and the nature of electron flow from the donor part to the acceptor group of the sensitizer. The complexity of the system also provides several

ways to improve the performance of the cell. For example, the introduction of the π-conjugated ring improves the stability as well as the performance of the sensitizer.[4] Additionally, improved electronic coupling between the lowest unoccupied molecular orbital of the sensitizer and conduction band of the semiconductor may improve charge transfer between the dye and titania.[5,6]

In DSSC only a monolayer of sensitizer is adsorbed on the semiconductor surface. Among the various proposed dyes, state-of-the-art ruthenium-based sensitizers have high-energy conversion efficiencies exceeding 11%.[7–9] However, the ruthenium based dyes are expensive and require very careful synthesis protocols and purification procedures.[10] To reduce the manufacturing cost of the DSSCs various metal free, organic sensitizers are now being proposed and investigated. These organic dyes are advantageous due to their tunable light absorption, higher molar extinction coefficient and the electrochemical properties.[10,11] An organic sensitizer usually is bestowed with a donor part (electron donating group), an acceptor part (electron accepting group) and a linker group. A number of donor groups have been investigated with varying success rates such as oligenes,[12–14] coumarins,[4,15–19] quinoxalines,[20,21] triphenylamine,[22–25] pyrrolidino,[26] and π-conjugated linker groups such as C-C double bonded chain,[12,14] thiophene units.[17,18,20,21,27,28] Inpartcular two types of acceptor/anchor groups, namely cyanoacrylic acid,[4,12–26] and carboxylic acid[27–29] are widely used in organic dye synthesis. Adsorption of sensitizers through carboxylic groups can take place either through chemisorption or physisorption.[30–34] The latter takes place via hydrogen bonding between the oxygen atom on TiO_2 surface

The SEC Strategic Research Cluster and the Centre for Synthesis and Chemical Biology, School of Chemical and Bioprocess Engineering, University College Dublin, Belfield, Dublin 4, Ireland; Tel: +353 1 716 1646; E-mail: niall.english@ucd.ie (N. J. English); Tel: +353 1 716 1995; Email: ravindranathan.thampi@ucd.ie (K. R. Thampi)

and the hydrogen atom of the carboxylic group of the dye. In chemisorptions, hydrogen atom from carboxylic acid dissociates and the bond is formed between carboxylic oxygen atoms and the surface titanium atoms of the oxide. Binding through chemisorption can be of monodentate ester, bidentate chelating or bidentate bridging types.[33,34] Experimental (ATR-FTIR) as well as theoretical studies for carboxylic acid adsorption on TiO$_2$ support chemisorption through bidentate bridging.[19,30,33,34]

Previous literature suggests[10] that coumarins demonstrate excellent electron donating ability. In addition, cyanoacrylic acid is widely used as an anchor/acceptor group and shows excellent charge withdrawing ability.[10] However, dyes with the coumarin donor and cyanoacrylic acceptor groups show different efficiencies[4] depending on the different linker groups employed. NKX-2311 and NKX-2593[4,15,35] (Figure 1) are coumarin based organic sensitizers with metheine unit (-CH=CH-) and thienylenevinylene unit in the linker, respectively, and cyanoacrylic acid as an acceptor/anchoring group. Introduction of a thiophene moiety in the metheine chain shows enhanced efficiency due to the extended π-conjugation in NKX-2593 sensitizer. The NKX-2311 and NKX-2593 dyes have their respective short-circuit current densities (J_{sc}) of 13.8 mAcm-2 and 14.7 mAcm-2, open circuit voltages (V$_{oc}$) 0.63 V and 0.67 V, fill factors 0.63 and 0.73 and efficiencies (η_{max}) 5.6% and 7.2% as reported previously.[4,15]

The overall efficiency of DSSCs may also change by the light absorption behavior of the sensitizers and sensitizer-surface complexes. The absorption ability of these systems at different light wavelengths contributes to the overall efficiency of the DSSCs and is a very important characteristic for the development of better DSSCs. Previous experimental reports[34,36–38] have shown that the deprotonation of carboxylic group of sensitizers during chemisorption on titania surface attributes to a blue shift in the absorption spectrum of the sensitizer-TiO$_2$ complex. The blue shift occurs due to the increase in the energy of the LUMO level of the dye as its proton is replaced by the metal ion of the titania.[37] On addition of acidic medium, a reprotonation of the carboxylate group (-COO$^-$) occurs and it displays a red shift in the absorption spectrum of the complex.[38] Therefore, in the present *in silico* study we investigate the effect of deprotonation of the carboxylate group on the light absorption behavior of the dye-surface complexes. We also investigate the effect of the introduction of thiophene moiety in the observed enhanced efficiency by NKX-2593, when compared to NKX-2311.

2 Computational Details

NKX-2311 and NKX-2593 sensitizers were modeled using Discovery Studio Visualizer package (Accelrys, San Diego, CA). For both dyes, the calculations were done using B3LYP
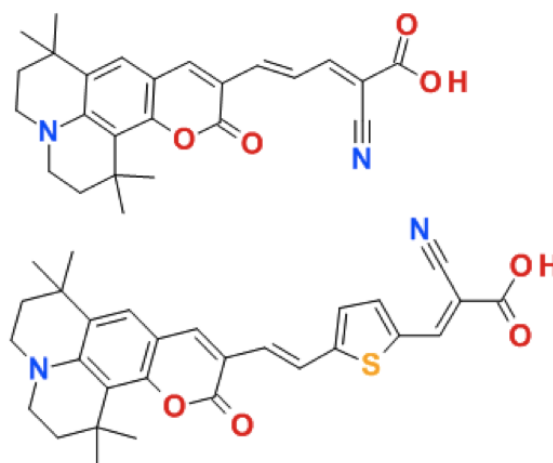

Figure 1 Schematic diagram of NKX-2311 (top) and NKX-2593 (bottom) dyes.

hybrid functional and 6-31G* basis set. The effects of the solvent (ethanol) were added using the polarizable continuum model of solvation (PCM)[39] as implemented in the Gaussian 09 software suit.[40] The optimized geometries are utilized to get the frontier orbitals and to carry out the time dependent density functional theory (TD-DFT) studies. We prepared a neutral, stoichiometric cluster of (TiO$_2$)$_{38}$ exposing anatase 101 surface as described by Persson et al[41]. Previous studies have shown that the (TiO$_2$)$_{38}$ cluster shows lowest excitation energy in good agreement with the experimental bandgap.[42,43] For geometry optimization, plane-wave DFT calculations were performed using projector augmented wave (PAW) pseudopotentials as implemented in the VASP package.[44,45] We carried out these calculations using generalized gradient approximation (GGA) of Perdew-Burke-Ernzerhof to account for the exchange-correlation effects.[46] An energy cutoff of 400 eV, and a Monkhorst-Pack k-point mesh[47] of 2 X 2 X 1 were used for geometry optimization and electronic property calculations. Both cell and atomic relaxations were carried out until the residual forces were below 0.01 eV/Å. Each dye-titania complex was separated from its images by addition of vacuum layers (>6 Å- thick) in the x- , y- and z- directions. VASP calculations were followed by single point TD-DFT calculations in ethanol solution using B3LYP functional together with a 6-31G* basis set in conjugation with PCM using Gaussian 09 software suit.[40]

3 Results and Discussion

3.1 NKX-2311 and NKX-2593 Dyes: Electronic Structures and Absorption spectrum

The optimized structures of the NKX-2311 and NKX-2593 sensitizers have planar geometries, as can be seen in Figure 2 and Figure 3. These figures also show the computed isodensity surfaces for the highest occupied molecular orbitals (HOMO) and lowest unoccupied molecular orbitals (LUMO). In both dyes, the HOMOs and LUMOs show π-character. While the HOMO is more or less delocalized over the entire dye molecule, LUMO is more localized on the cyanoacrylic acid anchor and linker groups. This is desirable and leads to the intramolecular charge separation upon excitation (push-pull effect). The change in electronic distribution between HOMO and LUMO is also indicative of a large dipole moment in the first excited state (as compared to the ground state)[24] and is the possible reason for the large oscillator strengths for the HOMO→LUMO transition as seen in Figure 4(a, d).

Figure 3 Molecular orbitals of NKX-2593 sensitizers relevant during photoexcitation. HOMO (top) and LUMO (bottom).
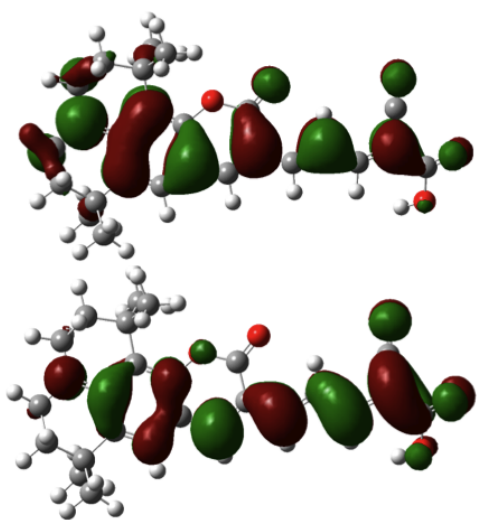

Figure 2 Molecular orbitals of NKX-2311 sensitizers relevant during photoexcitation. HOMO (top) and LUMO (bottom).

The experimental UV/Vis absorbance result in ethanol solution reported by Hara et al shows the absorption maximum (λ_{max}) at ~2.45 eV[4,15] for both NKX-2311 and NKX-2592 dyes. Our computational absorption spectrum for NKX-2311 and NKX-2593 in ethanol shows transition energies of high intensities, corresponding to the λ_{max} at 2.46 eV and 2.08 eV, (Table 1) respectively, as shown in Figure 4. The absorption spectrum of NKX-2593 shows another lower intensity absorption peak at 2.91 eV, resembling the peak present at ~3.26 eV in the experimental absorption spectrum.[4] This additional absorption peak for the NKX-2593 broadens its absorption spectrum. Here, the theoretically computed absorption energy for
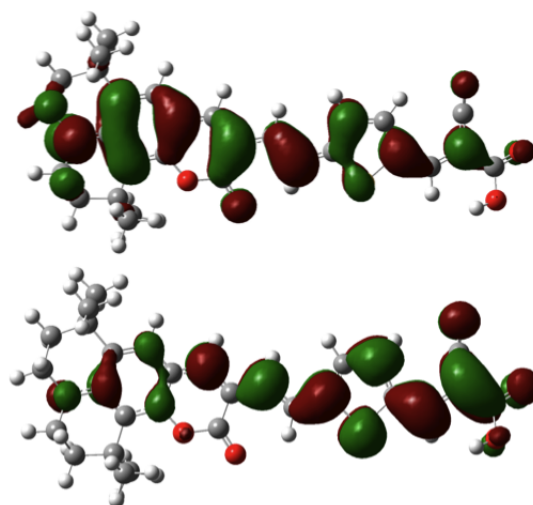
NKX-2311 is in total accord with the experimental absorption energy at λ_{max}. The computed absorption energy for NKX-2593 is slightly underestimated than the experimental results. This can be understood as follows: in the case of charge transfer transitions conventional exchange-correlation functionals like GGA and LDA do not contain the correct 1/R-dependence (R is the charge separation distance) and so fail to correctly predict the energies for charge transfer transition. This problem is partially remedied by hybrid functionals like B3LYP through the inclusion of exact exchange interaction. Although B3LYP improves the results but is still not perfect – at long range it goes as $0.2\,R^{-1}$ and not as R^{-1}. This results in an underestimation of the charge transfer transition energies. This error increases with increasing distance between charge donor and charge acceptor as is the case of NKX-2593.[24,48]

Isolated NKX-2311 dye has HOMO-LUMO gap (Δ_{HL}) of 2.59 eV while NKX-2593 dye shows HOMO-LUMO gap of 2.27 eV (Table 1). As expected, Δ_{HL} of NKX-2311 dye is slightly larger than that of NKX-2593 dye due to increased length of the latter dye. In DSSCs, the key process involves direct or indirect injection of the charge from the excited dye into the titania nanoparticle. So, the favorable placement of the HOMO and LUMO orbitals of the dye molecule relative to titania conduction band is important. As such, we also carried out the TD-DFT calculations for the isolated $(TiO_2)_{38}$ nanoparticle. We obtained HOMO-LUMO gap (Δ_{HL}) of 4.18 eV, with a TD-DFT lowest excitation energy of 3.49 eV (Table 1). The lowest excitation energy for computed TiO_2 cluster is in good agreement with the reported band gap value for TiO_2 nanoparticles of a few nm dimension.[49,50] Furthermore, HOMOs for both dyes are located within the TiO_2 bandgap and LUMOs are located at higher energy level com-
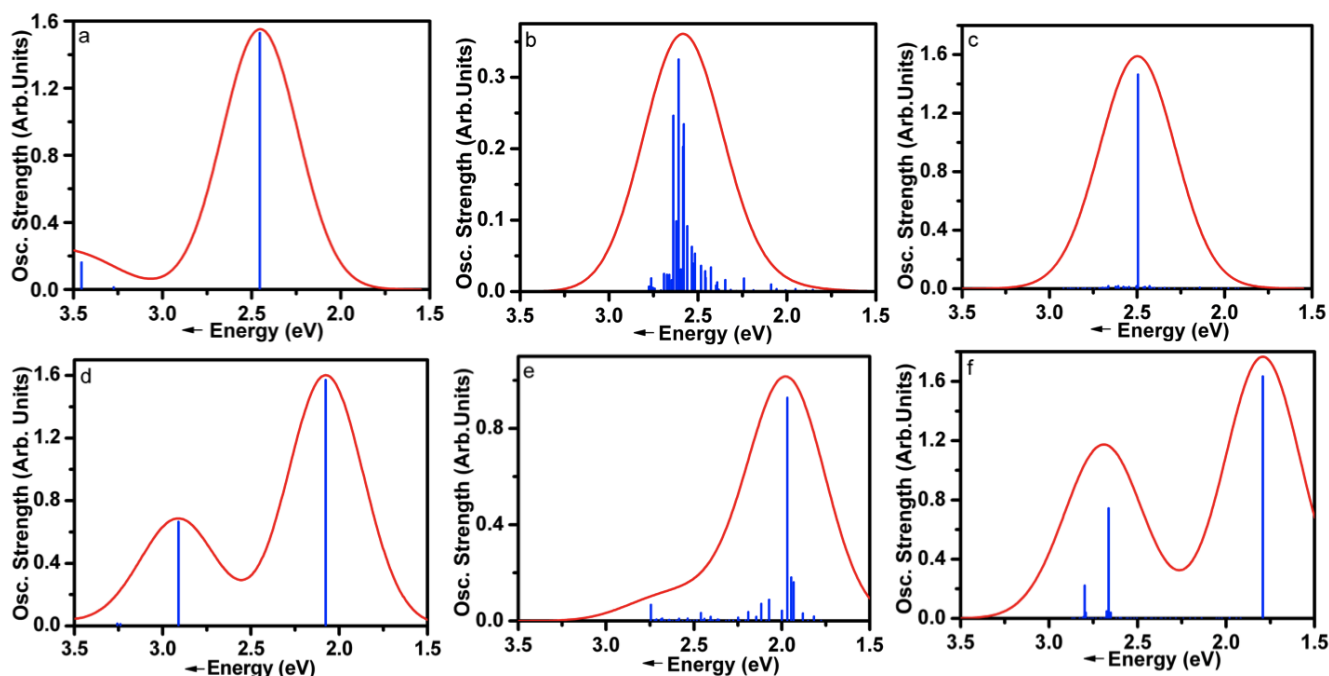
Figure 4 Calculated UV/Vis absorption spectra for a) NKX-2311, b) DP-2311/TiO2, c) P-2311/TiO$_2$, d) NKX-2593, e) DP-2593/TiO$_2$ and f) P-2593/TiO$_2$ complexes in ethanol solution. Blue represents oscillator strength and red represents gaussian fit with FWHM .5 eV.

Table 1 TD-DFT absorption energy (E) at λ_{max} corresponding HOMO (H), LUMO (L) energies and HOMO-LUMO gap (H - L = Δ_{HL}) of models

Systems	E (eV)	H (eV)	L (eV)	Δ_{HL} (eV)
NKX-2311	2.46	-5.33	-2.74	2.59
NKX-2311-DP	2.74	-4.97	-2.04	2.93
NKX-2593	2.08	-5.11	-2.84	2.27
NKX-2593-DP	2.44	-4.87	-2.18	2.69
TiO$_2$	3.49	-7.46	-3.28	4.18
P-2311/TiO$_2$	2.49	-5.31	-2.65	2.66
DP-2311/TiO$_2$	2.61	-5.20	-2.45	2.75
P-2593/TiO$_2$	1.79	-5.27	-3.30	1.97
DP-2593/TiO$_2$	1.96	-5.19	-3.00	2.19

Here, NKX-2311-DP and NKX-2593-DP are deprotonated dyes. P-2311/TiO$_2$ and P-2593/TiO$_2$ are protonated dyes adsorbed on titania and DP-2311/ TiO$_2$ and DP-2593/TiO$_2$ are deprotonated dye adsorbed on titania.

pared to the LUMO of isolated TiO$_2$ nanoparticle.

3.2 Dye-Titania Complexes: Electronic Structures and Absorption spectrum

In order to study the dye-titania complexes, we created the 114-atom titania nanoparticle, (TiO$_2$)$_{38}$, by exposing (101)-surface of the anatase titania.[31,41,42] The adsorption of various dyes on anatase (101) surface has been extensively studied, both experimentally and theoretically.[19,30–34,51] FT-IR study suggests that NKX-2311 sensitizer is adsorbed on TiO$_2$ surface through bidentate carboxylate mode[19] in which the carboxylate oxygen atoms bind to the Ti$_{5C}$ atoms exposed on titania surface. On the basis of these reports, we adopted the bidentate bridging mode for adsorption of both sensitizers on TiO$_2$ surfaces. To study the effects of the length of the linker group as well as the protonation vs. deprotonation of the dye upon adsorption, we created four structures. In the case of the protonated dyes, the hydrogen atom is kept bound with one of the carboxylic oxygen atoms and these complexes are named as P-2311/TiO$_2$ and P-2593/TiO$_2$. To create deprotonated dye-titania complex, the hydrogen atom is transferred from carboxylic acid to the surface oxygen of TiO$_2$. In rest of this work these complexes are referred to as DP-2311/TiO$_2$ and DP-2592/TiO$_2$.

The optimized geometries for the four complexes are given in Figure 5. The binding distances between carboxylate oxygen atoms and titanium atoms at the surface of DP-2311/TiO$_2$ complex are 2.07 and 2.15 Å . For DP-2593/TiO$_2$, these binding distances are 2.15 and 2.18 Å . This suggests a slightly stronger binding of the dye with the surface for DP-2311/TiO$_2$ compared to the DP-2593/TiO$_2$ complex. Compared to the deprotonated complexes, protonated P-2311/TiO$_2$ and P-2593/TiO$_2$ complexes show an increase in the binding distances. They are 2.32 and 2.44 Å for the former and
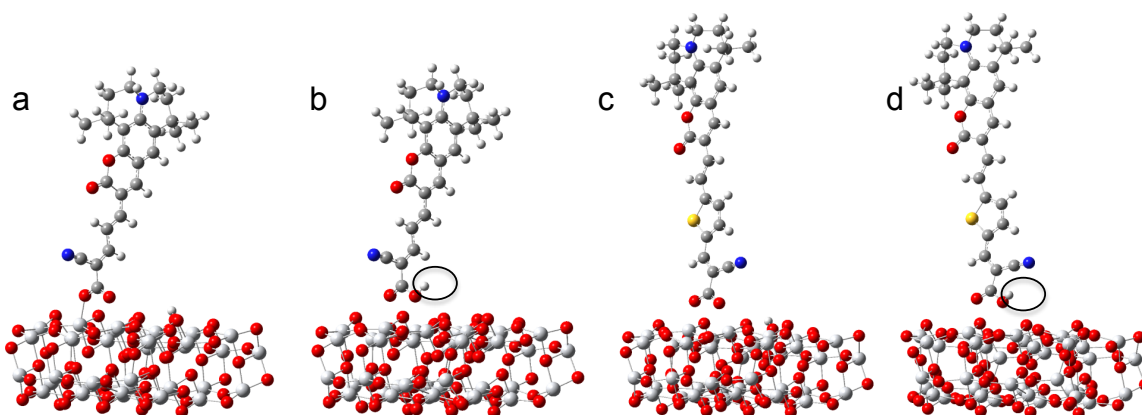
Figure 5 Optimized geometries for a) DP-2311/TiO$_2$ (b) P-2311/TiO$_2$ (c) DP-2933/TiO$_2$ (d) P-2593-TiO$_2$ complexes. Black circles indicate hydrogen atom attached with carboxylate group of dye.

Table 2 Transitions corresponding to λ_{max} and a few comparative peaks.

System Excitation State:	Transition energy (eV) (Oscillator strength (f))	Wave function (Coefficients)
NKX-2311		
1:	2.45 (1.53)	H→L (0.71)
DP-2311/TiO$_2$		
34:	2.54 (0.23)	H→L+32 (0.11), H→L+33 (0.24), H→L+34 (0.30), H→L+35 (0.49), H→L+36 (-0.23), H→L+38 (-0.14)
35:	2.58 (0.20)	H→L+32 (0.13), H→L+33 (0.61), H→L+34 (-0.13), H→L+35 (-0.12), H→L+36 (0.24)
37:	2.61 (0.33)	H→L+33 (-0.16), H→L+35 (0.31), H→L+36 (0.58), H→L+37 (-0.12)
39:	2.64 (0.25)	H→L+35 (0.13), H→L+38 (0.62), H→L+39 (0.28)
P-2311/TiO$_2$		
21:	2.49 (1.46)	H→L+18 (0.42), H→L+19 (0.56)
NKX-2593		
1:	2.08 (1.57)	H→L (0.71)
2:	2.91 (0.67)	H-1→L (0.51), H→L+1(-0.48)
DP-2593/TiO$_2$		
5:	1.93 (0.16)	H→L+4 (0.68), H→L+7 (0.16)
6:	1.94 (0.18)	H→L+5 (0.66), H→L+7 (-0.21)
7:	1.96 (0.93)	H→L+4 (-0.16), H→L+5 (0.21), H→L+6 (0.22), H→L+7 (0.60), H→L+8 (-0.15)
P-2593/TiO$_2$		
1:	1.79 (1.63)	H→L (0.71)
32:	2.66 (0.74)	H-2→L (0.15), H-1→L (0.56), H→L+30 (0.15), H→L+31 (-0.16), H→L+55 (-0.10), H→L+58 (-0.13), H→L+59 (0.15), H→L+60 (-0.16)

2.48 and 2.50 Å for the latter structure. Among protonated-dye/surface complexes P-2311/TiO$_2$ again shows smaller binding distances compare to P-2593/TiO$_2$ complex. Furthermore smaller binding distances for deprotonated-dye/surface complexes than protonated-dye/surface complexes favors adsorption of deprotonated dyes. Here, favorable binding of carboxylate group over carboxylic group with TiO$_2$ surface could be due to an extra electron of the carboxylate-oxygen that can be shared with the under-coordinated titanium atom.

The experiment done on NKX-2311/TiO$_2$ complex in ethanol by Hara *et al* [15] shows slight blue shift as well as a broadening of the absorption peak [FWHM=∼.5 eV(∼2.3 eV - ∼2.8 eV)] relative to the isolated dye. Figure 4 shows the calculated UV/Vis spectrum for the dye-titania complexes in ethanol solution. DP-2311/TiO$_2$ has an absorption band that extends from ∼2.2 - 2.8 eV with the peak at 2.61 eV (λ_{max}), which is in agreement with the experimental results. The calculated band contains several excitations, with the most important transitions (highest oscillator strengths) listed in Table 2. All these transitions take place from the HOMO of the complex which is mostly localized on the dye and retains the HOMO character of the isolated dye (Figure 6a(i)). The unoccupied states involved in the transition extend from LUMO+32 to LUMO+39. In most of these important excitations, LUMO+36 shows considerable involvement and has the largest contribution at λ_{max}. Figure 6a(ii) is an isosurface plot of LUMO+36 showing contributions to it from both the dye and the titanium dioxide. All unoccupied orbitals below LUMO+32 shows contribution only for surface with no dye character [see Figure 7 (col. 1)]. On the other hand, the three highest occupied MOs (HOMO to HOMO-2) show localization only on dye. This was verified by visualization of these MOs.

In contrast to the case of deprotonated dye-titania complex, the absorption spectrum of P-2311/TiO$_2$ has only one major excitation for λ_{max} at 2.49 eV. The excitation shows contribution form HOMO→LUMO+18 and HOMO→LUMO+19 only (Table 2). Among them, LUMO+19 shows major contribution in the excitation and is delocalized over the linker and acceptor moieties of the dye as well as on titania (Figure 6b(ii)). The unoccupied orbitals below LUMO+18 are localized to the titania nanoparticle only. Similar to DP-2311/TiO$_2$ complex, HOMO to HOMO-2 show only dye character. This is also indicated in Figure 7 (col. 3). In the case of DP-2311/TiO$_2$, the gap between HOMO and LUMO+36 is 2.75 eV (Figure 7, col. 1). For P-2311/TiO$_2$ complex, the gap between the MOs involved in the highest intensity transition is 2.66 eV (Figure 8, col. 3). The results from excited state calculation for DP-2311/TiO$_2$ and P-2311/TiO$_2$ complexes show a blue shift in the absorbance spectrum of the former complex as compared to the latter.
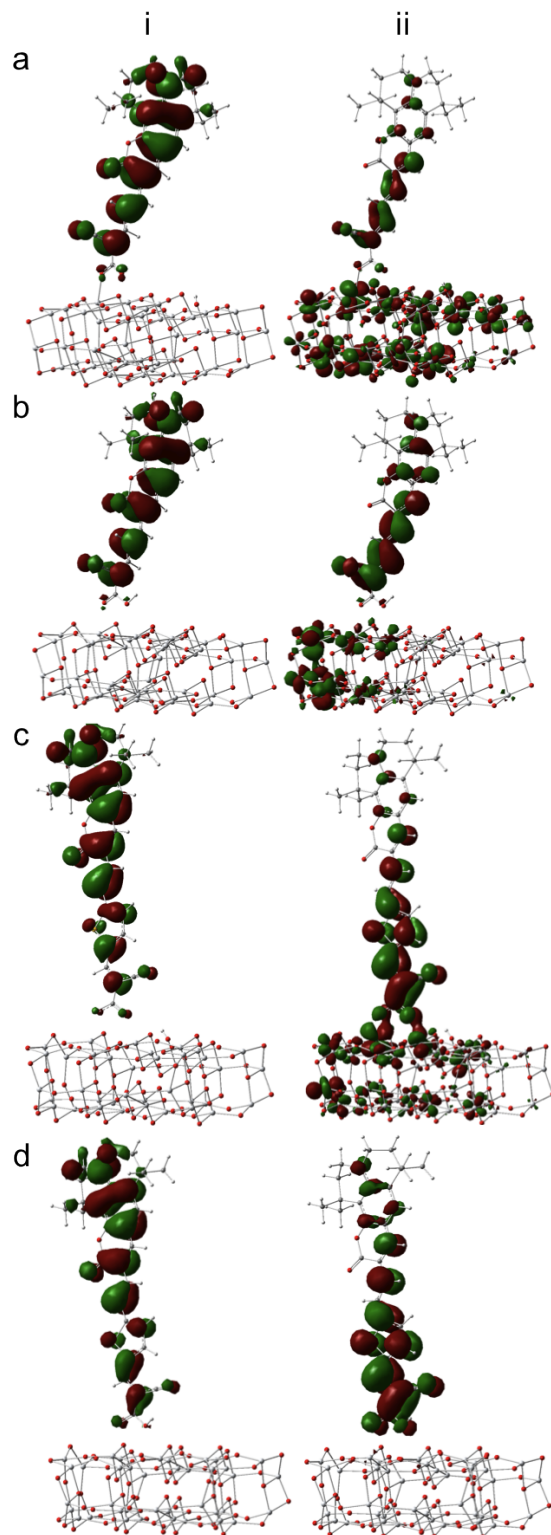
An experimental study performed by Hara's group [35] on

Figure 6 Molecular orbitals relevant during photoexcitation for (a) DP-2311/TiO$_2$ (i) HOMO (ii) LUMO+36 (b) P-2311/TiO$_2$ (i) HOMO (ii) LUMO+19 (c) DP-2593/TiO$_2$ (i) HOMO (ii) LUMO+7 (d) P-2593-TiO$_2$ (i) HOMO (ii) LUMO complexes .
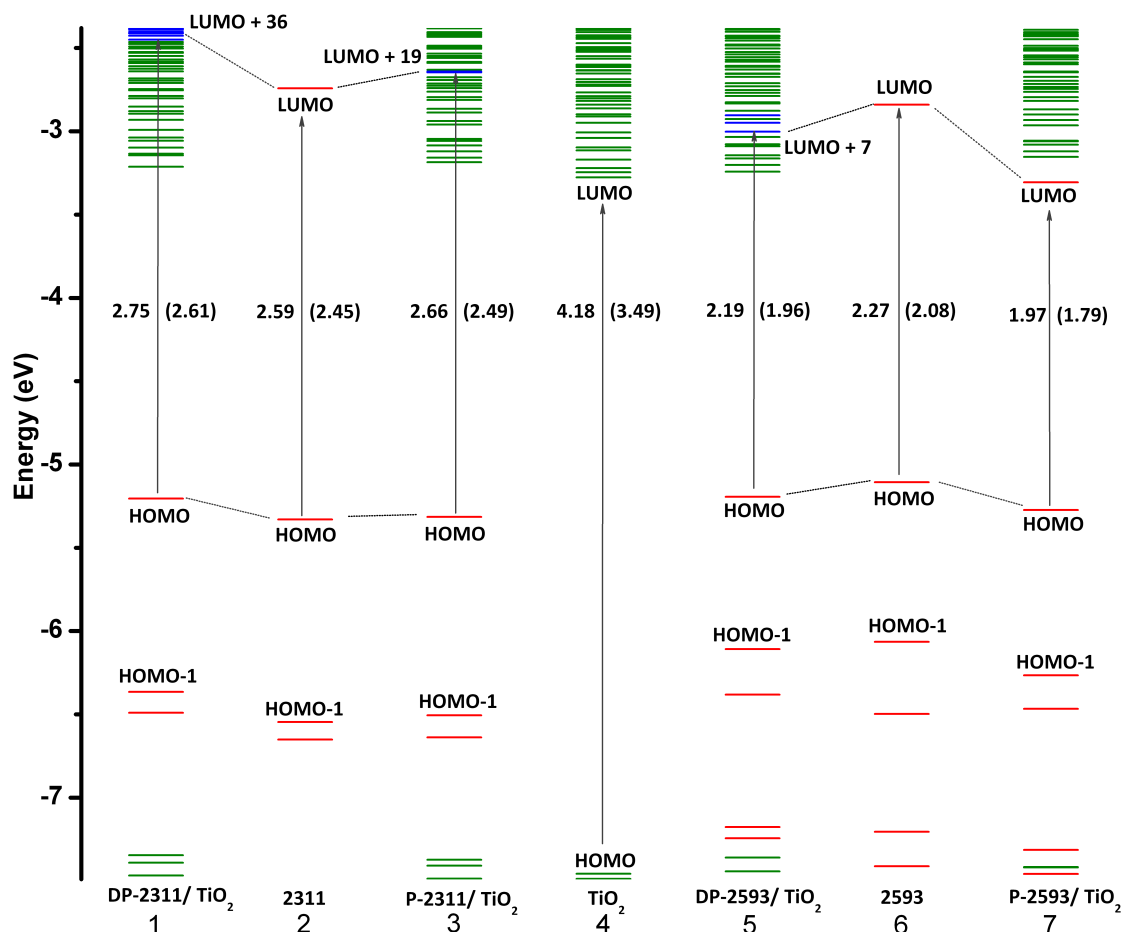
Figure 7 Schematic molecular orbital energy level (eV) diagram of isolated NKX-2311 sensitizer (2311) (col. 2) and NKX-2593 sensitizer (2593)(col. 6), interacting DP-2311/TiO$_2$ (col. 1), P-2311/TiO$_2$ (col. 3), DP-2593/TiO$_2$ (col. 5) and P-2593/TiO$_2$ complex (col. 7), and isolated TiO$_2$ (col. 4) systems in ethanol solution. Green represents states localized on TiO$_2$. Red represents states localized on sensitizers. Blue represents states localized on dye and surface. Values in parenthesis refer to the TD-DFT excitation energies.

NKX-2593/TiO$_2$ in ethanol shows a blue shift as well as broadening of absorption peak [FWHM = ∼0.8 eV (∼2.3 - ∼3.1 eV)] compared to the isolated dye. DP-2593/TiO$_2$ complex shows computed absorption band expends from ∼1.7 - ∼2.4 eV with peak at 1.96 eV and a slight shoulder at ∼2.7 eV. Here mainly three excited states contributed in the transition with high oscillator strengths and they are listed in table 2. The HOMO and LUMO+7 contribute in all three transitions. The LUMO+7 state is an admixture of π^* orbitals of the dye and the empty states derived mainly from d-orbitals of titanium [Figure 6c(ii)]. Here, LUMO+7 is delocalized over the entire thiophene ring, deprotonated cyanoacrylic acid anchor and continues over to the titania nanoparticle attached to the anchor. The delocalization of LUMO demonstrates a strong coupling between the dye and the interface at the oxide surface. Figure 7, col. 5 shows that the energy gap between the HOMO and LUMO+7 is 2.19 eV. All unoccupied states below the LUMO+7 are localized only on titania. These localized states are represented in green color in Figure 7 (col. 5). The five highest occupied MOs are localized mostly on the dye [shown in red in Figure 7 (col. 5)].

The computed P-2593/TiO$_2$ complex shows maximum absorbance at ∼1.79 eV (Figure 6d). The only state contributed to this excitation is HOMO→LUMO (Table 2). LUMO of the complex shows resemblance with unoccupied orbital of isolated dye with negligible surface contribution from titania (Figure 6d(ii)). The top four occupied MOs in P-2593/TiO$_2$ (Figure 7, col. 7) complex are derived mostly from the dye. HOMO and LUMO are located at -5.27 eV and -3.30 eV respectively with Δ_{HL} of 1.97 eV. Figure 6d shows another low intensity absorption peak at ∼2.66 eV. This transition comes from the excitation between HOMO-2 and LUMO+60. With

the exception of LUMO, the unoccupied orbital are localized on the titania nanoparticle (Figure 7, col. 7).

It is interesting to note that the two protonated complexes show excitations at lower energies (i.e. at higher wavelengths) compared to the deprotonated complexes (Table 1). In order to understand the origin of this blue shift, we also calculated the absorption spectrum for the individual deprotonated dyes (NKX-2311-DP and NKX-2593-DP) (Table 1). In this calculation, the dyes had a net charge of $-|e|$. Both deprotonated dyes show a blue-shift in their spectrum when compared to the protonated dyes. We also observed that the HOMO and LUMO energies for deprotonated dyes have shifted to higher energies when compared to the respective protonated dyes (Table 1). Our theoretical results are in agreement with the experimental data.[34,36–38] As discussed in the introduction, these experiments also report a blue shift in the spectrum of the complexes as compared to the noninteracting dyes. This shift is attributed to the deprotonation of the cyanoacrylic acid, leading to a weaker electron accepting ability of the resulting carboxylate/TiO$_2$ complex.[36]
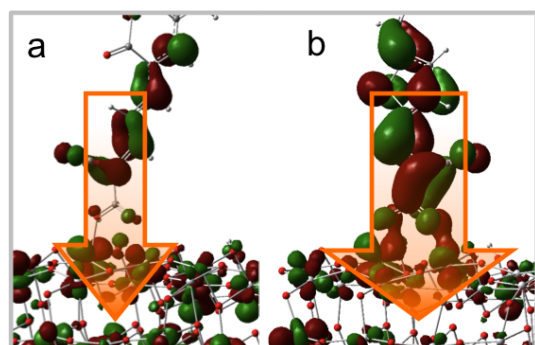

Figure 8 Relative probability density at dye's anchor and titania interface for (a) DP-2311/TiO$_2$ (b) DP-2593/TiO$_2$ complexes. The larger arrow reflects the experimentally observed increase in J_{sc} with the increase in the charge density.

Among all the four dye/TiO$_2$ complexes studied, the deprotonated-dye/surface complexes show better delocalization of LUMO at anchor/surface interface than the protonated-dye/surface complexes. A recent study has shown that the short circuit current, J_{sc}, is directly related with the probability density at anchor moiety.[52] This is also supported by Wang *et al* [53] who showed an increased photocurrent with an increase in the electronic coupling between dye and titania surface. As discussed in the introduction, J_{sc} for NKX-2593/TiO$_2$ complex is better than that of NKX-2311/TiO$_2$ complex, which is reflected in our computed probability densities for DP-2593/TiO$_2$ and DP-2311/TiO$_2$ complexes (Figure 8). The unoccupied orbital involved in the transition corresponding to λ_{max} for DP-2593/TiO$_2$ complex also suggests better hybridization of surface and dye orbitals as compared

to the DP-2311/TiO$_2$ complex and is a possible reason for the improved short-circuit current densities for the former system. The placement of the excited states in the conduction band of the respective complexes as well as their isosurface plots can throw light on the mechanism involved in the electron injection from the excited dye to titania. For DP-2593/TiO$_2$, DP-2311/TiO$_2$ and P-2311/TiO$_2$ complexes, direct electron transfer can be the mechanism responsible for the injection of the electron into titania. This is due to the improved electronic coupling between the lowest unoccupied molecular orbital of the dye and conduction band of the semiconductor. For all the three systems MOs near LUMO are localized only on surface, which can accept charge from higher unoccupied MOs involved in the transition. In the case of P-2593/TiO$_2$ complex, the two peaks in the absorption spectrum have different characters. The higher intensity peak at 1.70 eV corresponds HOMO - LUMO transition, where both MOs are localized on the dye. This transition will not result in charge injection into titania. For this reason we have investigated the lower intensity peak at 2.66 eV. The orbitals involved in this transition are mostly localized on the titania nanoparticle. In this case, one expects that the injection mechanism is direct transfer of the charge (upon excitation) from the dye to titania.

4 Conclusions

In this work we carried out a detailed DFT/TD-DFT calculation for the two coumarin sensitizers in isolated and in complexation modes with anatase (101) nanoparticle. The calculations were done for both protonated and deprotonated forms of the anchor moiety. The introduction of longer π-conjugated linker in NKX-2593 increases the charge separation between donor and acceptor moieties and hinders the possibility of charge recombination in the dye. Our results show that NKX-2593/TiO$_2$ complexes also exhibit red shift in the absorption spectrum compared to the NKX-2311/TiO$_2$ complexes. The red shift in the former complex reflects better stabilization of dye and titania MOs due to hybridization than the latter complex. This could be a contributing factor to the better performance of NKX-2593 over NKX-2311 dye. The TD-DFT results suggest that both dye exhibit direct charge transfer to titania due to excitation. Further, this study confirms that deprotonation of carboxylic acid (anchor moiety) during adsorption on surface leads to the experimentally observed blue shift in the absorption spectrum compared to the case of the protonated anchor moiety.

5 Acknowledgements

authors wish to thank Ritwik Kavathekar for his useful contribution in the scientific discussions. The authors also thank Dr. Run Long for his discussion regarding VASP software.

References

1 B. O'Regan and M. Grätzel, *Nature*, 1991, **353**, 737–740.
2 M. Grätzel, *J Photochem. Photobio. C: Photochem. Reviews*, 2003, **4**, 145.
3 J. H. Yum, P. Chen, M. Grätzel and M. K. Nazeeruddin, *ChemSusChem*, 2008, **1**, 699–707.
4 K. Hara, M. Kurashige, Y. Dan-oh, C. Kasada, A. Shinpo, S. Suga, K. Sayama and H. Arakawa, *New Journal of Chemistry*, 2003, **27**, 783–785.
5 M. Miyashita, K. Sunahara, T. Nishikawa, Y. Uemura, N. Koumura, K. Hara, A. Mori, T. Abe, E. Suzuki and S. Mori, *J Am Chem Soc*, 2008, **130**, 17874–81.
6 M. Pastore and F. D. Angelis, *ACS Nano*, 2009, **4**, 556–562.
7 M. Grätzel, *Journal of Photochemistry and Photobiology A: Chemistry*, 2004, **164**, 3–14.
8 M. K. Nazeeruddin, F. De Angelis, S. Fantacci, A. Selloni, G. Viscardi, P. Liska, S. Ito, B. Takeru and M. Grätzel, *J Am Chem Soc*, 2005, **127**, 16835–47.
9 M. K. Nazeeruddin, A. Kay, I. Rodicio, R. Humphrybaker, E. Muller, P. Liska, N. Vlachopoulos and M. Grätzel, *J Am Chem Soc*, 1993, **115**, 6382–6390.
10 A. Mishra, M. K. Fischer and P. Bauerle, *Angew Chem Int Ed Engl*, 2009, **48**, 2474–99.
11 F. M. H. Tian, *Organic Photovoltaics: Mechanisms, Materials, and Devices*, Eds.: S.-S. Sun, N. S. Sariciftci, CRC, London,, 2005.
12 K. Hara, M. Kurashige, S. Ito, A. Shinpo, S. Suga, K. Sayama and H. Arakawa, *Chem Commun (Camb)*, 2003, 252–3.
13 K. Hara, T. Sato, R. Katoh, A. Furube, T. Yoshihara, M. Murai, M. Kurashige, S. Ito, A. Shinpo, S. Suga and H. Arakawa, *Advanced Functional Materials*, 2005, **15**, 246–252.
14 T. Kitamura, M. Ikeda, K. Shigaki, T. Inoue, N. A. Anderson, X. Ai, T. Lian and S. Yanagida, *Chemistry of Materials*, 2004, **16**, 1806–1812.
15 K. Hara, K. Sayama, Y. Ohga, A. Shinpo, S. Suga and H. Arakawa, *Chemical Communications*, 2001, 569–570.
16 K. Hara, Y. Tachibana, Y. Ohga, A. Shinpo, S. Suga, K. Sayama, H. Sugihara and H. Arakawa, *Solar Energy Materials and Solar Cells*, 2003, **77**, 89–103.
17 K. Hara, Z. S. Wang, T. Sato, A. Furube, R. Katoh, H. Sugihara, Y. Dan-Oh, C. Kasada, A. Shinpo and S. Suga, *J Phys Chem B*, 2005, **109**, 15476–82.
18 K. Hara, K. Miyamoto, Y. Abe and M. Yanagida, *J Phys Chem B*, 2005, **109**, 23776–8.
19 K. Hara, T. Sato, R. Katoh, A. Furube, Y. Ohga, A. Shinpo, S. Suga, K. Sayama, H. Sugihara and H. Arakawa, *J. Phys. Chem. B*, 2003, **107**, 597–606.
20 R. K. Chen, X. C. Yang, H. N. Tian and L. C. Sun, *Journal of Photochemistry and Photobiology a-Chemistry*, 2007, **189**, 295–300.
21 R. K. Chen, X. C. Yang, H. N. Tian, X. N. Wang, A. Hagfeldt and L. C. Sun, *Chemistry of Materials*, 2007, **19**, 4007–4015.
22 W. Xu, B. Peng, J. Chen, M. Liang and F. Cai, *Journal of Physical Chemistry C*, 2008, **112**, 874–880.
23 W. H. Liu, I. C. Wu, C. H. Lai, P. T. Chou, Y. T. Li, C. L. Chen, Y. Y. Hsu and Y. Chi, *Chem Commun (Camb)*, 2008, 5152–4.
24 D. P. Hagberg, T. Marinado, K. M. Karlsson, K. Nonomura, P. Qin, G. Boschloo, T. Brinck, A. Hagfeldt and L. Sun, *J Org Chem*, 2007, **72**, 9550–6.
25 K. R. J. Thomas, Y. C. Hsu, J. T. Lin, K. M. Lee, K. C. Ho, C. H. Lai, Y. M. Cheng and P. T. Chou, *Chemistry of Materials*, 2008, **20**, 1830–1840.
26 P. Qin, X. Yang, R. Chen, L. Sun, T. Marinado, T. Edvinsson, G. Boschloo and A. Hagfeldt, *The Journal of Physical Chemistry C*, 2007, **111**, 1853–1860.
27 S. Tan, J. Zhai, H. Fang, T. Jiu, J. Ge, Y. Li, L. Jiang and D. Zhu, *Chemistry*, 2005, **11**, 6272–6.
28 K. Tanaka, K. Takimiya, T. Otsubo, K. Kawabuchi, S. Kajihara and Y. Harima, *Chemistry Letters*, 2006, **35**, 592–593.
29 J.-H. Yum, P. Walter, S. Huber, D. Rentsch, T. Geiger, F. Nüesch, F. De Angelis, M. Grätzel and M. K. Nazeeruddin, *Journal of the American Chemical Society*, 2007, **129**, 10320–10321.
30 J. Ahdjoudj and C. Minot, *Catalysis Letters*, 1997, **46**, 83–91.
31 M. Pastore and F. De Angelis, *ACS Nano*, 2010, **4**, 556–562.
32 A. Vittadini, A. Selloni, F. P. Rotzinger and M. Grätzel, *The Journal of Physical Chemistry B*, 2000, **104**, 1300–1306.
33 K. Srinivas, K. Yesudas, K. Bhanuprakash, V. J. Rao and L. Giribabu, *Journal of Physical Chemistry C*, 2009, **113**, 20117–20126.
34 M. K. Nazeeruddin, R. Humphry-Baker, P. Liska and M. Grätzel, *The Journal of Physical Chemistry B*, 2003, **107**, 8981–8987.
35 Z.-S. Wang, Y. Cui, Y. Dan-oh, C. Kasada, A. Shinpo and K. Hara, *The Journal of Physical Chemistry C*, 2008, **112**, 17011–17017.
36 L.-Y. Lin, C.-H. Tsai, K.-T. Wong, T.-W. Huang, L. Hsieh, S.-H. Liu, H.-W. Lin, C.-C. Wu, S.-H. Chou, S.-H. Chen and A.-I. Tsai, *The Journal of Organic Chemistry*, 2010, **75**, 4778–4785.
37 Z.-S. Wang and H. Sugihara, *Langmuir*, 2006, **22**, 9718–9722.
38 D. P. Hagberg, T. Edvinsson, T. Marinado, G. Boschloo, A. Hagfeldt and L. Sun, *Chemical Communications*, 2006, 2245–2247.
39 M. Cossi, G. Scalmani, N. Rega and V. Barone, *The Journal of Chemical Physics*, 2002, **117**, 43–54.
40 M. J. Frisch, G. W. Trucks, H. B. Schlegel, G. E. Scuseria, M. A. Robb, J. R. Cheeseman, G. Scalmani, V. Barone, B. Mennucci, G. A. Petersson, H. Nakatsuji, M. Caricato, X. Li, H. P. Hratchian, A. F. Izmaylov, J. Bloino, G. Zheng, J. L. Sonnenberg, M. Hada, M. Ehara, K. Toyota, R. Fukuda, J. Hasegawa, M. Ishida, T. Nakajima, Y. Honda, O. Kitao, H. Nakai, T. Vreven, J. A. Montgomery, Jr., J. E. Peralta, F. Ogliaro, M. Bearpark, J. J. Heyd, E. Brothers, K. N. Kudin, V. N. Staroverov, R. Kobayashi, J. Normand, K. Raghavachari, A. Rendell, J. C. Burant, S. S. Iyengar, J. Tomasi, M. Cossi, N. Rega, J. M. Millam, M. Klene, J. E. Knox, J. B. Cross, V. Bakken, C. Adamo, J. Jaramillo, R. Gomperts, R. E. Stratmann, O. Yazyev, A. J. Austin, R. Cammi, C. Pomelli, J. W. Ochterski, R. L. Martin, K. Morokuma, V. G. Zakrzewski, G. A. Voth, P. Salvador, J. J. Dannenberg, S. Dapprich, A. D. Daniels, O. Farkas, J. B. Foresman, J. V. Ortiz, J. Cioslowski and D. J. Fox, *Gaussian 09 Revision A.1*, Gaussian Inc. Wallingford CT 2009.
41 P. Persson, R. Bergstrom and S. Lunell, *The Journal of Physical Chemistry B*, 2000, **104**, 10348–10351.
42 F. De Angelis, A. Tilocca and A. Selloni, *Journal of the American Chemical Society*, 2004, **126**, 15024–15025.
43 F. De Angelis, *Chemical Physics Letters*, 2010, **493**, 323–327.
44 G. Kresse and J. Hafner, *Phys. Rev. B*, 1993, **47**, 558.
45 G. Kresse and J. Furthmüller, *Comput. Mat. Sci.*, 1996, **6**, 15.
46 J. P. Perdew, K. Burke and M. Ernzerhof, *Physical Review Letters*, 1996, **77**, 3865–3868.
47 H. J. Monkhorst and J. D. Pack, *Phys. Rev. B*, 1976, **13**, 5188.
48 A. Dreuw and M. Head-Gordon, *Chemical Reviews*, 2005, **105**, 4009–4037.
49 M. Khoudiakov, A. R. Parise and B. S. Brunschwig, *Journal of the American Chemical Society*, 2003, **125**, 4637–4642.
50 Y.-X. Weng, Y.-Q. Wang, J. B. Asbury, H. N. Ghosh and T. Lian, *The Journal of Physical Chemistry B*, 1999, **104**, 93–104.
51 R. Sánchez-de-Armas, M. San-Miguel, J. Oviedo and J. F. Sanz, *Computational and Theoretical Chemistry*, 2011,

doi:10.1016/j.comptc.2011.01.010,.

52 R. Jose, A. Kumar, V. Thavasi, K. Fujihara, S. Uchida and S. Ramakrishna, *Applied Physics Letters*, 2008, **93**, 23125–3.

53 F. De Angelis, S. Fantacci, A. Selloni, M. Grätzel and M. K. Nazeeruddin, *Nano Letters*, 2007, **7**, 3189–3195.